Materials Today Chemistry 23 (2022) 100720

Contents lists available at ScienceDirect

Materials Today Chemistry

journal homepage: www.journals.elsevier.com/materials-today-chemistry/

Tendon-bone junction healing by injectable bioactive thermo-sensitive hydrogel based on inspiration of tendon-derived stem cells

K. Huang [a, c], J. Du [b, c], J. Xu [a, c], C. Wu [a], C. Chen [a], S. Chen [b], T. Zhu [b, ***], J. Jiang [a, **], J. Zhao [a, *]

[a] Department of Sports Medicine, Department of Orthopedics, Shanghai Jiao Tong University Affiliated Sixth People's Hospital, Shanghai 200233, PR China
[b] Frontier Institute of Medical & Pharmaceutical Science and Technology, School of Chemistry and Chemical Engineering, Shanghai University of Engineering Science, Shanghai 201620, PR China

ARTICLE INFO

Article history:
Received 7 October 2021
Received in revised form
17 November 2021
Accepted 26 November 2021
Available online xxx

Keywords:
Methylcellulose
KGN
Mesoporous bioactive glass nanoparticles
Chronic rotator cuff tears
Tendon-bone junction

ABSTRACT

The rotator cuff repaired construct must establish a contiguous and functioning tendon-bone junction to provide adequate stability. However, fibrocartilage deficiency and bone loss were hardly reversed after physical suture, especially in chronic rotator cuff tears. In this study, we synthesized an injectable methylcellulose/polyvinyl alcohol/polyvinylpyrrolidone-based thermo-sensitive hydrogel, which delivered kartogenin-loaded mesoporous bioactive glass nanoparticles. Physicochemical studies the revealed phase transition temperatures of 35 °C and its ability to induce chondrogenesis and osteogenesis differentiation of tendon-derived stem cells. Furthermore, experiments in rabbit chronic rotator cuff tears model confirmed the fibrocartilage and bone layer regenerative capability of the injected bioactive hydrogel, which could, in turn, support the ultimate tensile stress of the repaired rotator cuff. The bioactive agents-loaded hydrogel reported in this study is a valuable addition to the arsenal of biomaterials in applications to chronic tendon-bone junction injuries.

1. Introduction

Rotator cuff tears (RCTs) is the most common reason for shoulder pain and reduced mobility, which contributes to >250,000 repair surgeries every year in America alone [1]. The retear rate ranges from 20% in adult patients to 94% in aged patients [2,3] because of poor healing of the tendon-bone junction (TBJ). Abrupt transition leads to the 'functional grading' between the TBJ, where the gradual variation of composition and structure result in mechanical properties to alleviate stress concentrations [4,5]. However, once the TBJ is injured, scar healing is mostly observed rather than fibrocartilage or mineralized fibrocartilage-based healing [6]. In the meantime, long-term mechanical unloading in chronic RCTs is usually accompanied by a bone loss at the interface [7], which often leads to loosening/pulling out of the anchor, resulting in failure of the surgical intervention [8]. Several tissue engineering strategies were developed, including the nanofiber scaffold, biochemical cues, even stem cells were involved, but to our knowledge, few studies solve problems of both bone and cartilage lineage simultaneously [5].

Considering the narrow space between tendon and bone, the injectable thermosensitive hydrogels show numerous advantages over conventional therapeutics, based on their fluidity and ability to form material *in situ* [9]. Methylcellulose (MC) was well known for its thermoreversible gelation characteristics, with intermolecular hydrogen bonds forming a cage-like structure [10]. It was approved by the Food and Drug Administration for its biocompatible and used for ophthalmic drug delivery [11]. Different additives like polymers or various salts could alter the lower critical solution temperature (LCST) of MC [12,13]. Appropriate application of polyvinyl alcohol (PVA) and NaCl will reduce the LCST to around 45 °C [14]. Because the MC/PVA-based hydrogels hardly meet the mechanical strength requirements in shoulder joint repair, the addition of polyvinylpyrrolidone (PVP) is useful in stabilizing the network via the formation of inter-chain hydrogen bonding [15], which also plays a role in decreasing the LCST of MC [16].

* Corresponding author.
** Corresponding author.
*** Corresponding author.
E-mail addresses: zhutonghe89@163.com (T. Zhu), jessicajj19@hotmail.com (J. Jiang), jzzhao@sjtu.edu.cn (J. Zhao).
[c] These authors contributed equally to this work.

https://doi.org/10.1016/j.mtchem.2021.100720
2468-5194/

There is an urgent need in developing both bone and cartilage inducing biochemical cues for complex transitional organs. Recently, tendon-derived stem cells (TDSCs) were isolated from edges of the torn rotator cuff and have been reported to have the ability to differentiate into cells of multiple lineages [17,18]. Application of tissue engineering technology for enhanced osteogenesis and chondrogenesis of TDSCs can potentially lead to improved TBJ-based self-repair. Kartogenin (KGN) was proved to promote robust chondrocyte differentiation of BMSCs [19] and has shown advantages in fibrocartilage formation or collagen organization after rotator cuff repair [20]. Functional groups activated mesoporous bioactive glass nanoparticles (MBGs) were popular in bone tissue engineering applications and were found to stimulate the proliferation and differentiation of BMSCs [21]. Thus far, a combination of KGN and MBGs has not been tried before. KGN could be grafted to NH_2-BG because of the free carboxyl group. We hypothesized that KGN and MBGs will work together and solve the fibrocartilage deficiency and bone loss problems in chronic RCTs.

In this study, we prepared an injectable thermosensitive MC/PVA/PVP hydrogel which carried a composite of KGN@MBGs. This hydrogel could self-heal at body temperature and construct a KGN-MBGs constant release environment *in situ*. The TBJ regeneration performance *in vivo* was investigated in a rabbit model with chronic RCTs after injection. TDSCs bi-lineage inducing capability of the hydrogel were confirmed *in vitro* (Scheme 1). The aim of this study was to induce local reconstruction of specific TBJ tissue after the repair of chronic RCTs.

2. Materials and methods

2.1. Materials

MC M450, tetraethyl orthosilicate (TEOS, 98%), calcium nitrate ($Ca(NO_3)_2 \cdot 4H_2O$, 99%), ethanol (99.7%), triethyl phosphate (TEP, 99.8%), DMSO were purchased from Sinopharm Chemical Reagent Co. Ltd. PVP (K30), PVA, hexadecyl trimethyl ammonium bromide (CTAB), ammonia aqueous (NH_4OH), 3-aminopropyltriethoxysilane (APTES, ≥98%), 1-ethyl-3-(3-dimethylaminopropyl) carbodiimide hydrochloride (EDCI), N-Hydroxysulfosuccinimide sodium salt (SNHS) were provided by Sigma-Aldrich Co. Ltd. LIVE/DEAD™ Cell Imaging Kit, KGN, Dulbecco's Modified Eagle Medium (DMEM), αMEM, fetal bovine serum (FBS), and phosphate-buffered saline (PBS) were obtained from Thermo Fisher Scientific Co. Ltd. Chondrogenic and osteogenic differentiation medium (DM) were purchased from Sciencell Co. Ltd. Antibody of Collagen 1, bone morphogenetic protein 2 (BMP2), Runx2, Sox9, Collagen 2 and Aggrecan were acquired from Bioss Biotechnology Co., Ltd. Dyeing kits of Alizarin red S and Alcian blue were procured from Solarbio Technology Co. Ltd. Type I collagenase and dispase was purchased from Worthington Biochemical Co. Ltd and Stem cell Technologies Inc separately.

2.2. Fabrication of KGN@MBGs

2.2.1. Synthesis of MBGs-NH_2

MBGs-NH2 was prepared as described in previous studies [22,23]. Bioactive glasses were modulated using the sol-gel

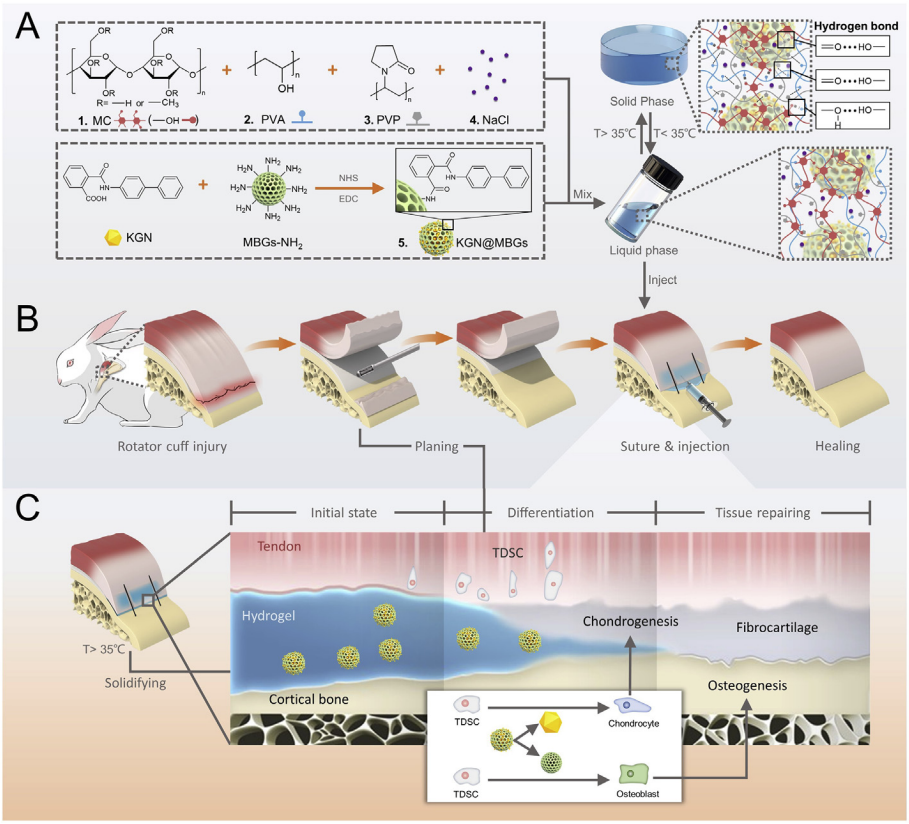

Scheme 1. KGN@MBGs thermosensitive hydrogels for regeneration of tendon-bone junction in chronic rotator cuff tears model. (**A**) The construction and mechanism of bioactive hydrogels. (**B**) Rabbit chronic rotator cuff tears model establishment, repair, and injection. (**C**) Bi-lineage inducing functions provided by hydrogels, satisfying the regeneration of tendon-bone healing. KGN, kartogenin; MBG, mesoporous bioactive glass nanoparticle.

method. To put it simply, 5.6 g CTAB was dissolved in a mixed solution containing ddH_2O (25 mL) and ethanol (80 mL), heated to 40 °C, and stirred continuously until completely dissolved. Respectively, 9.4 mL ammonia, 15.23 mL TEOS, and 1.58 mL TEP were added in turn, 30 min stirring was then followed. After adding 9.62 g calcium nitrate and stirring for 3 h, the white precipitate was separated from the glass sol after centrifugation. Finally, the BGs product was obtained by drying in the oven for 24 h and then sintering in the Muffle furnace (550 °C, 6 h). The prepared 6 g bioactive glass was added to the mixed solution containing 3 mL double-distilled water (ddH_2O) and 200 mL ethanol. After ultrasonic dispersion of 30 min, 6 mL APTES was dropped into the solution. Following stirring at 65 °C for 6 h, the system was washed with ddH_2O and ethanol. The product was then dried overnight in a vacuum drying oven at 60 °C, and MBGs-NH2 was obtained.

2.2.2. Grafting MBGs-NH2 with KGN to form KGN@MBGs

KGN was grafted to free amines, as our previous study described [24]. Totally 32 mg KGN was dissolved in 3 mL DMSO. Then 3 mL KGN/DMSO solution, 0.13 mmol EDC, and 0.07 mmol NHS were added to 29 mL PBS, respectively. The mixed solution was stirred for 5 h to activate the carboxyl group of KGN. 200 mg prepared MBGs-NH2 was added to the previously activated KGN solution and stirred. After the covalent reaction at room temperature for 48 h, the stent was cleaned with a large amount of ddH_2O to remove the by-products adsorbed on the surface.

2.2.3. Fabrication of thermosensitive hydrogel and system integration

The MC/PVA/PVP thermosensitive hydrogel was synthesized based on previous studies and improvements were made [25–27]. Totally 260 mg MC was added into 12.2 mL ddH_2O at 70 °C and stirred continuously until it was uniformly dispersed. The MC solution was prepared by placing it in the refrigerator for 48 h. After dissolving 200 mg NaCl in 2 mL ddH_2O at room temperature, it was added into MC solution and stirred to form a mixed solution. According to the grouping, three different components were added to the system: ①simple hydrogel group: 2 mL ddH2O; ②KGN/Gel group: 2 mL ddH2O that dissolved 6.4 mg KGN; ③KGN@MBGs/Gel group: 2 mL H2O that contained 46.4 mg KGN@MBGs. Then 260 mg PVP was added to the mixed solution and stirred evenly. Subsequently, 4 mL 5% PVA solution was added and stirred evenly. Thus, we got the three groups of thermosensitive hydrogel with or without biochemical cues. The concentrations of KGN in the hydrogels were both 320 μg/mL and that of BGs were 2 mg/mL.

2.3. Characterization of the hydrogel

2.3.1. Rheological measurement

The oscillatory sweep experiments of hydrogel were accomplished using advanced rheometer (TA Instrument, model AR 2000) using a cone and plate geometry. The cone angle was 1° and the diameter was 75 mm. The device is equipped with a temperature unit (Peltier plate), which can effectively control the temperature (±0.05 °C) over an extended time within the temperature range considered in this work. The dynamic viscoelastic functions, including shear storage modulus (G′) and loss modulus (G″), were measured as the function of time and temperature. To determine the sol-gel point, the angular frequency (ω) was set at interval 1–10 rad/s, the heating rate was set at 1 °C/min from 10 °C to 50 °C, and strain amplitude (γ) was set at 0.03, so as to minimize the perturbation to the network during the gel evolution [28]. The data obtained were analyzed using rheology advantage data analysis software.

2.3.2. Transmission electron microscopy

Transmission electron microscopy (TEM) was performed to observe the size of bioactive glasses in the hydrogels. Hydrogel samples were diluted with ddH_2O in the proportion of 1:5, then dispersed in an ultrasonic bath for 10 min. A small volume (3–5 μL) of suspension was dropped onto the carbon-coated copper grids and recorded in the Zeiss-Leo 906E TEM.

2.3.3. Fourier transform infrared spectroscopy

The attenuated total reflectance method was used with a Nicolet 6700 spectrometer (Thermo, USA) in the range 4000-800 cm^{-1}. A total of 36 scans were collected with an absorption mode of 2 cm^{-1}, and the average spectrum was obtained.

2.3.4. In vitro release study

One milliliter samples of KGN/Gel and KGN@MBGs/Gel were injected into dialysis bags and placed in 15 mL PBS solution, respectively. Three replicates were made for each group. The release study was carried out in a shaker at 37 °C and 100 rpm. The solution was changed with the same volume of phosphate buffer at each predetermined time points after centrifugation. The KGN concentration was determined by high performance liquid chromatography (Agilent 1260 Infinity II, USA) and analyzed at 274 nm using a C-18 chromatographic column (150 × 4.6 mm, 5 mm). The MBGs degeneration products were calculated by Ca^{2+} level with inductively coupled plasma atomic emission spectrometry (Perkin-Elmer Optima 7000DV) [29].

2.4. In vitro experiments

2.4.1. Extraction and culture of TDSCs

TDSCs were derived, cultured and identified according to published studies [30]. The experimental protocol was approved by the local Institutional Animal Care and Use Committee. 3-Weeks-old female Sprague-Dawley rats were included, and Achilles tendons were collected. 3 rats were used at a time. After tendon sheath and surrounding tissues were removed, tendons were cut into small pieces (1–2 mm^3). Every 100 mg of tissue was digested by 3 mg/mL type I collagenase and 4 mg/mL dispase in 1 mL PBS at 37 °C for 1 h. After centrifugation at 1500g for 15min, digested tissues were suspended in DMEM containing 10% FBS and 1% Penicillin-Streptomycin (P–S), then cultured at 37 °C with 5% CO_2. After 5 days, the loosened tissue residues were removed by exchanging the medium. 0.25% trypsin/EDTA was used for cell passaging.

For identification, surface markers of adherent cells were detected through flow cytometry performed by FACSCalibur (BD Biosciences, USA). The cells (5×10^5) were isolated with 0.05% trypsin/EDTA and washed with PBS containing 3% FBS, following suspended in a 50 μL buffer containing 3% FBS and incubated 30 min with fluorescence-labeled monoclonal antibodies against CD31, CD45, CD90, CD105 (Invitrogen, USA) in the dark at 4 °C. CD90 and CD105 are markers of mesenchymal stem cells, while CD31 and CD45 are markers of non-hematopoietic cells. Nonspecific mouse PE-conjugated IgG (BD Bioscience, USA) was used as homotype control. After incubation, the cells were washed twice and then suspended in 500 μL PBS containing 3% FBS for flow cytometry detection. FlowJo software (Tree Star, USA) was used to analyze the data and results were shown in Fig. S1.

Tri-lineage differentiation was carried out for stem cell confirmation on the other hand. Adipogenesis differentiation was induced by low-glucose Dulbecco's modified Eagle's medium with 100 nM dexamethasone, 0.5 mM isobutyl-1-methylxanthine, and 50 μM indomethacin for 3 weeks. Oil Red O staining was performed after fixation (Fig. S2). The osteogenic and chondrogenic induction method was described in 2.4.3.

2.4.2. Cells culture with hydrogels and live-dead assay

It was difficult for the hydrogels to stay in the solid condition at room temperature during experiments. A 6-well transwell chamber (Nest Biotechnology, China) equipped with the polyester membrane (PET, pore diameter of 8 μm) was used for culturing and inducing of TDSCs [31]. Cells were seeded in the bottom well with a density of 1×10^4 cells, and 1 mL hydrogel was spread evenly on the upper chamber. 1 mL PBS was added to the chamber in the blank group for control.

After co-culture for 1 day and 5 days, the LIVE/DEAD™ Cell Imaging Kit was used for biocompatibility test of hydrogels. The cells were incubated with 500 μL working solution per well for 20 min at room temperature and then observed with fluorescence microscopy (ZEISS, AxioImager M1, Germany).

2.4.3. In vitro cell induction

Osteogenic and chondrogenic differentiation was conducted with hydrogels for cell induction property confirmation. Generation 2 or 3 of TDSCs were used. After confluency, the culture medium was changed to DM, and transwell chambers with different hydrogels (1 mL) were placed to form the co-culture system. 1 mL PBS was added to the chamber for control.

The osteogenic DM contains αMEM with 10% FBS, 50 μg/mL vitamin C and 4 mM β-glycerophosphate. The medium was changed every 72 h. The protein expression level of collagen I, Runx2, and BMP2 were detected by Western blotting (WB) on the 14th day. After 14 days of induction, cells were fixed with 4% (v/w) paraformaldehyde and stained with alizarin red. Light microscope (X7, Olympus, Japan) was used for observation. For semi-quantitative, cells were later destained with 60% isopropanol. The absorbance of the extracted pigment was determined at 510 nm (TECAN).

The chondrogenic DM contains αMEM with 1% insulin transferrin selenium solution, 1 mM sodium pyruvate, 50 μg/mL ascorbic acid, 40 μg/mL L-proline, 100 nM dexamethasone, and 10 ng/mL TGF-β3. For WB detection, the procedure of cell treatment is the same as that of osteogenic induction, and expression levels of Sox9, collagen 2, and Aggrecan were detected. The medium was changed every day for 7 days. A further experiment of a 3D pellet system was used for chondro inductive ability confirmation. Briefly, 1×10^6 cells were resuspended with 1 mL chondrogenic medium in a 15 mL centrifugal tube and centrifuged at 250 g for 5min. After two days' culture and cells came into a pellet, move the pellet to the co-culture system in the plate. Frozen

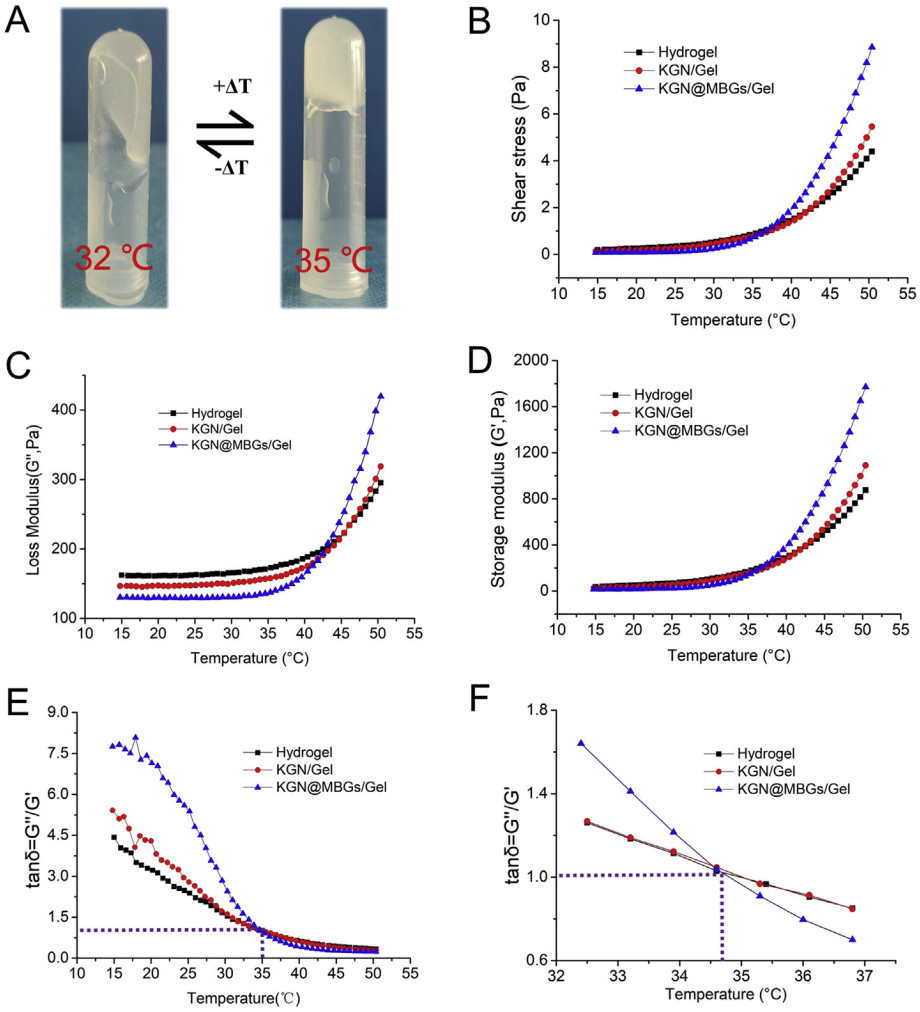

Fig. 1. Rheological properties of hydrogels. (**A**) Reversible phase transition hydrogels when temperature fluctuates. (**B**), (**C**), (**D**): The storage modulus (G′), loss modulus (G″) curve and shear stress with respect to temperature through rheological test. (**E**) The tan δ (=G″/G′) curve used for sol-gel point observation. (**F**) It was around 35 °C when tanδ = 1.

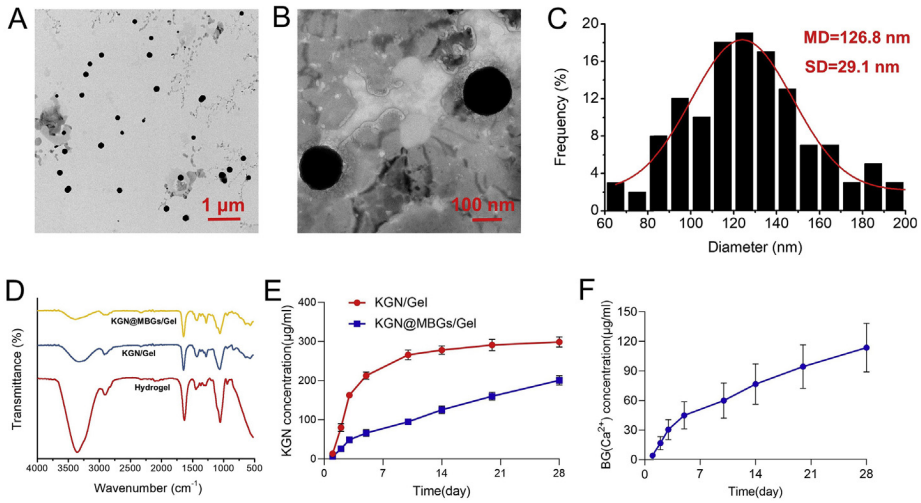

Fig. 2. TEM observation of BGs in large field (**A**) and detailed version (**B**). (**C**) Diameter distribution of BGs with mean value of 126.76 ± 30.29 nm. (**D**) FTIR spectra of hydrogels. (**E**) The release curve of KGN from KGN/Gel and KGN@MBGs/Gel. (**F**) The release curve of BGs (Ca^{2+}) from KGN@MBGs/Gel. KGN, kartogenin; MBG, mesoporous bioactive glass nanoparticle; TEM, transmission electron microscopy.

section and Alcian blue staining was carried out after 21 days of differentiation. Bern score system (Table S1) was used for the evaluation of the pellet [32].

2.5. In vivo experiments

2.5.1. Rabbit model establish and repair of chronic RCTs

All animal experimental procedures were approved by the Institutional Animal Care and Use Committee (IACUC) of Shanghai Jiao Tong University Affiliated Sixth People's Hospital. Chronic RCTs models were established and repaired according to protocols of previous studies in rabbits [33,34]. 130 male New Zealand rabbits with the age of 4 months old were included in this study. 120 of them were used for chronic RCTs repair; another 10 rabbits were used for confirmation of the successful establishment of the chronic RCTs model. After rabbits were anesthetized with pentobarbital (30 mg/kg), 125 supraspinatus tendons were detached from the greater tuberosity of the humerus and marked with suture rings, while the other five were not. The distal end of the tendon was wrapped with a 10 mm-long silicon Penrose drain to prevent adhering to surrounding tissues (Fig. S3). Then close the incisions and wait for 8 weeks till the chronic RCTs model was carried out. 5 rabbits with or without rotator cuff surgery were sacrificed. Micro-computed tomography was arranged for bone loss evaluation in the greater tuberosity. Oil red O staining was used for confirmation of lipid infiltration in supraspinatus muscle (Fig. S4).

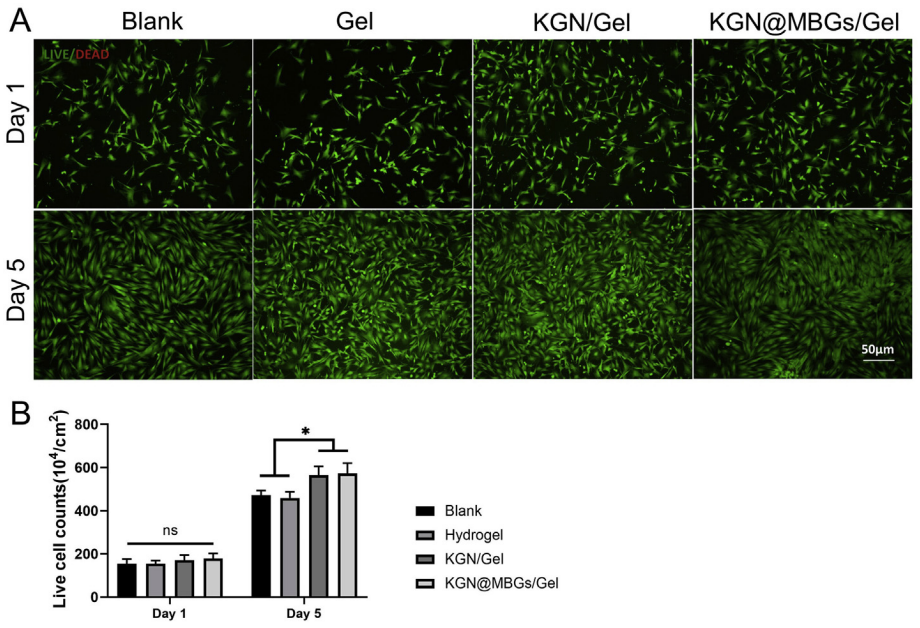

Fig. 3. Live/Dead staining result of TDSCs co-culturing with hydrogels by transwell chamber. (**A**) Fluorescence images of live (green) and dead (red) TDSCs are co-cultured with PBS (Blank), simple hydrogel (Gel), KGN/Gel, and KGN@MBGs/Gel for 1 day and 5 days. (**B**) Live cells count the result of the Live/Dead staining. (ns = no significance, *P < 0.05, n = 3). KGN; kartogenin; MBG, mesoporous bioactive glass nanoparticle; TDSC, tendon-derived stem cell.

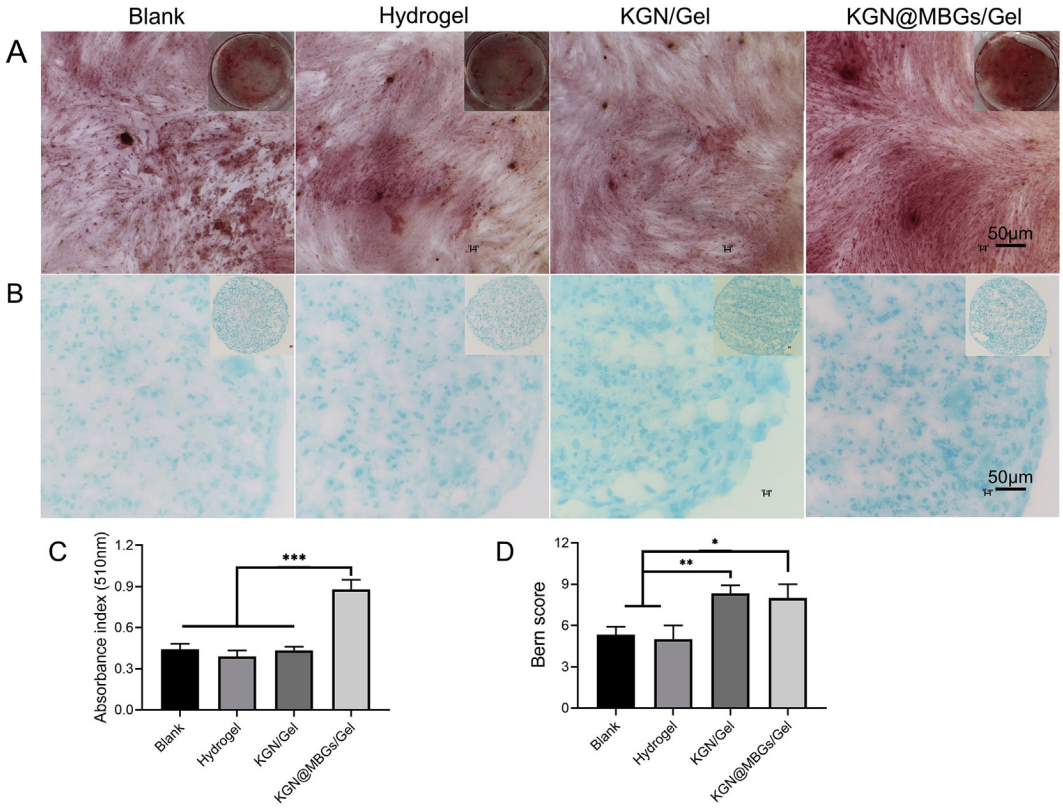

Fig. 4. *In vitro* confirmation of osteogenesis and chondrogenesis inducing ability. (**A**) Alizarin red staining results of TDSCs after osteogenesis induction with different hydrogels. (**B**) Alcian blue staining results of the pellets after chondrogenesis induction of TDSCs with different hydrogels. (**C**) Absorbance index of Alizarin red staining at 510 nm. (**D**) Histological evaluation of the pellets with Bern score system. (*P < 0.05, **P < 0.01, ***P < 0.001, n = 3). TDSC, tendon-derived stem cell.

For rotator cuff repair and hydrogel injection, 120 rabbits were randomly divided into 4 groups. Following footprint preparation and tendon fixation with a double transosseous tunnel created by hand drill ($\Phi = 2$ mm), three different hydrogels (200 μL) were injected in bone tunnel and TBJ. An equal volume of PBS was injected for control. At 1, 2, and 3 months after repair surgery, 10 rabbits from each group were sacrificed and humerus-supraspinatus complexes were obtained, with 5 used for histological investigation of bone and fibrocartilage regeneration, and another 5 for the biomechanical test to detect the strength.

2.5.2. Micro-CT analysis

The microstructure of bone healing condition was observed by micro-CT (SkyScan 1176, Bruker, German), particularly the bone tunnel used for tendon fixation. The scanning procedure was set at 80 kV, 450 mA with a layer thickness of 18 μm. A customized

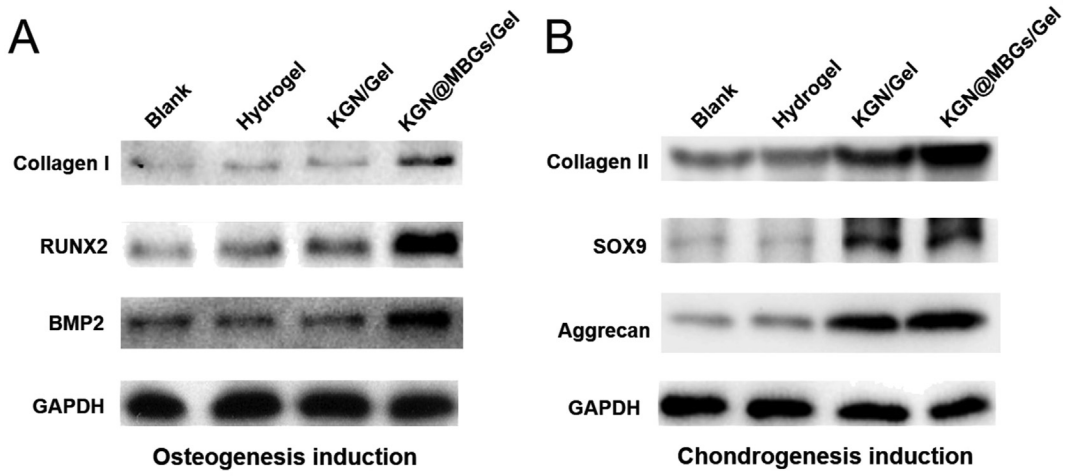

Fig. 5. The protein expression of TDSCs related to osteogenesis and chondrogenesis process. (**A**) Collagen I, Runx2, and BMP2 expression after osteogenic induction. (**B**) Collagen II, Sox9, and Aggrecan expression after chondrogenic induction. TDSC, tendon-derived stem cell.

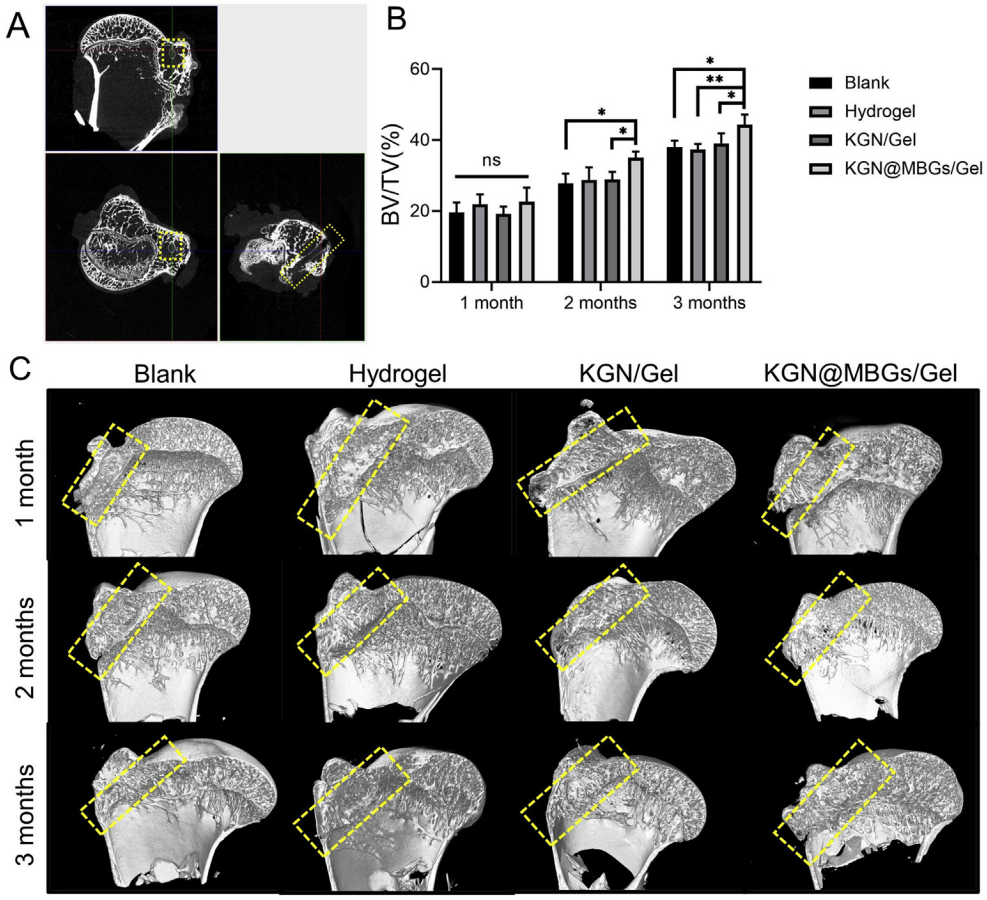

Fig. 6. Bone tunnel healing condition observed by micro-CT. (**A**) Bone tunnel explanation in sagittal, axial and oblique axial view. (**B**) BV/TV statistical results of the bone tunnel after repair with different hydrogels for 1, 2, and 3 months. (**C**) Interior view of the tunnel for observation of new generated trabecular bone. (*P < 0.05, **P < 0.01, n = 5). BV, bone volume; TV, total volume.

cylindrical region of interest with a diameter of 1 mm, which was created by hand drill, was determined for bone volume fraction (bone volume/total volume, BV/TV) calculation.

2.5.3. Fibrocartilage layer staining

Safranin O-fast green staining, Alcian blue staining, and type II collagen immunostaining were used for cartilage observation in the interface between tendon and bone. After micro-CT scanning, specimens were fixed in 4% paraformaldehyde for 2 days, followed by decalcified, wrapped, and cut into slices for histological staining. In short, for Safranin O-fast green staining, slices were drenched in Safranin O for 4 min, washed in running water, and dyed in the fast green dye for 4 min. Then washed with ddH_2O and glacial acetic acid solution for 1–2 min sequently. The chondroitin sulfate in fibrocartilage would be stained as red. For Alcian blue staining, slices were stained in Alcian blue solution for 3–5 h and then neutralized in the saturated borax solution for 2 d. The acid mucopolysaccharide within fibrocartilage would be stained in blue. For type II collagen immunostaining, slices were blocked in 3% bovine serum albumin solution at room temperature for 30min, incubated in Col II antibody solution at 4 °C overnight, immersed in the second antibody at room temperature for 1 h, and visualized in 3,3 N-diaminobenzidine tertrahydrochloride solution. Images were captured with a microscope (Leica, Germany).

2.5.4. Biomechanical test

The mechanical stability of supraspinatus and humerus complex after rotator cuff repair was detected through the biomechanical test. Sixty shoulders were selected for biomechanical evaluation (5 in each group and each time point). After the supraspinatus tendon-humerus complex was isolated from the shoulder of rabbits, the cross-sectional area of the attachment area of the supraspinatus tendon was measured with a digital caliper. All specimens are kept in a −80 °C freezer until biomechanical tests are performed (MTS, USA). The humeral shaft was firmly embedded in the polyvinyl chloride cylinder, while the supraspinatus tendon was wrapped in polyester cloth and woven with a No.2 Ethibond suture to prevent the pinching injury of the tendon. Tendon was fixed vertical to the humeral shaft, according to the functional position of the supraspinatus tendon. The loading speed was set at 0.5 mm/min until the ultimate load to failure of the supraspinatus tendon-humerus complex was recorded [35]. The results of ultimate load, ultimate stress, and stiffness are processed and analyzed by OriginPro software (OriginLab, USA).

2.6. Statistical analysis

All results were represented as the mean ± standard deviation (SD). One-way ANOVA and Tukey's tests were used for difference evaluation by Origin Pro 8. If the normal distribution and equal

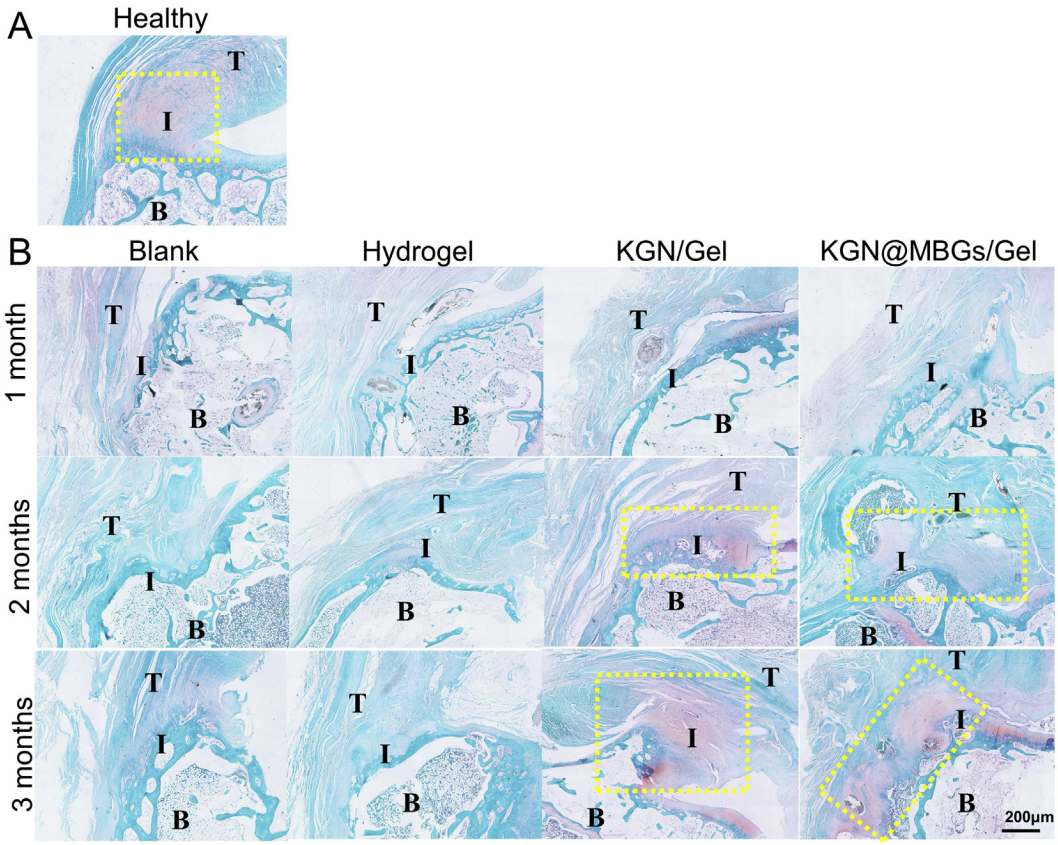

Fig. 7. Safranin O-fast green staining results of the interface of tendon-to-bone. (**A**) Healthy interface presented abundant cartilage layer (red) between tendon and bone. (**B**) Regeneration of cartilage layer after repair without hydrogel, or with simple hydrogel, KGN/Gel and KGN@MBGs/Gel for 1, 2 and 3 months. (T = tendon; B = bone; I = interface; the yellow box labeled the fibrocartilage area.). KGN, kartogenin; MBG, mesoporous bioactive glass nanoparticle.

variance were not met, Kruskal-Wallis test was performed to verify data like load-to-failure values. The significance level was set at a value of 0.05.

3. Results

3.1. Characterization of the hydrogels

The sol-gel point was initially tested using a thermostat water bath, and the gelation temperature of all hydrogels were around 35 °C. The gelation time was about 45s in 35 °C to form a solid-like gel (Fig. 1A). Three hydrogels showed no significant difference in gelation property.

Further rheological experiment revealed the detail of the gelation procedure. The G′, G″ and shear stress were tested as the temperature rose gradually (Fig. 1B–D). According to the method of Winter [36], a frequency-independent value of tan δ (=G″/G′) could be used for gelation temperature which tan $\delta = 1$. Thus the sol-gel points which were around 35 °C could be observed directly in Fig. 1D–F.

Morphology of BGs was observed through TEM after centrifugation and concentration. As shown in Fig. 2A–B, the BGs were uniform spherical nanoparticles surrounded with hydrogels. The diameters were in a normal distribution with a mean value of 126.76 nm and a standard deviation of 30.29 nm. Fig. 2C shows the Fourier transform infrared spectra of hydrogels; peaks at 3361 cm^{-1} and 1051 cm^{-1} were attributed to the hydrogen bonds among the hydrogels. It is difficult to distinguish the KGN@MBGs signal because the –CO–NH- band also exists in PVP, which shows an absorption peak at 1640 cm^{-1}. Release curves of KGN from KGN/Gel and KGN@MBGs/Gel were shown in Fig. 2E, respectively. The release concentration was calculated using the ratio of the released KGN amount to the volume of hydrogels. The KGN/Gel group exhibited a more rapid release profile than KGN@MBGs/Gel group because of the free KGN molecules. While the release of KGN in KGN@MBGs/Gel was related to hydrolysis or the degeneration of BGs. Fig. 2F showed the release curve of Ca^{2+} from the BGs. Releasing of Ca^{2+} is bound to be accompanied by Si delivering, both of which are proposed to facilitate osteogenesis [37].

3.2. Cytocompatibility assay

Biocompatibility was confirmed through Live/Dead staining after TDSCs co-culturing with three groups of hydrogels in transwell chambers for 1 day and 5 days (Fig. 3). Few dead cells (red) were observed in hydrogel groups, and no significance was found in cells counts compared with the blank group on 1st day. KGN/Gel and KGN@MBGs/Gel groups showed more live cells after being cultured for 5 days. No significant difference was found between the blank and simple hydrogels groups. This phenomenon indicated low or non-toxicity of the MC-based hydrogel, and biochemical cues in it enhanced the proliferation ability of TDSCs.

3.3. In vitro osteogenesis and chondrogenesis inductive capabilities

The osteogenesis and chondrogenesis induction was conducted to verify the inductive capabilities of KGN@MBGs/Gel. Fig. 4A showed the alizarin red staining results of TDSCs after osteogenic induction with PBS, simple hydrogel, KGN/Gel, and KGN@MBGs/Gel

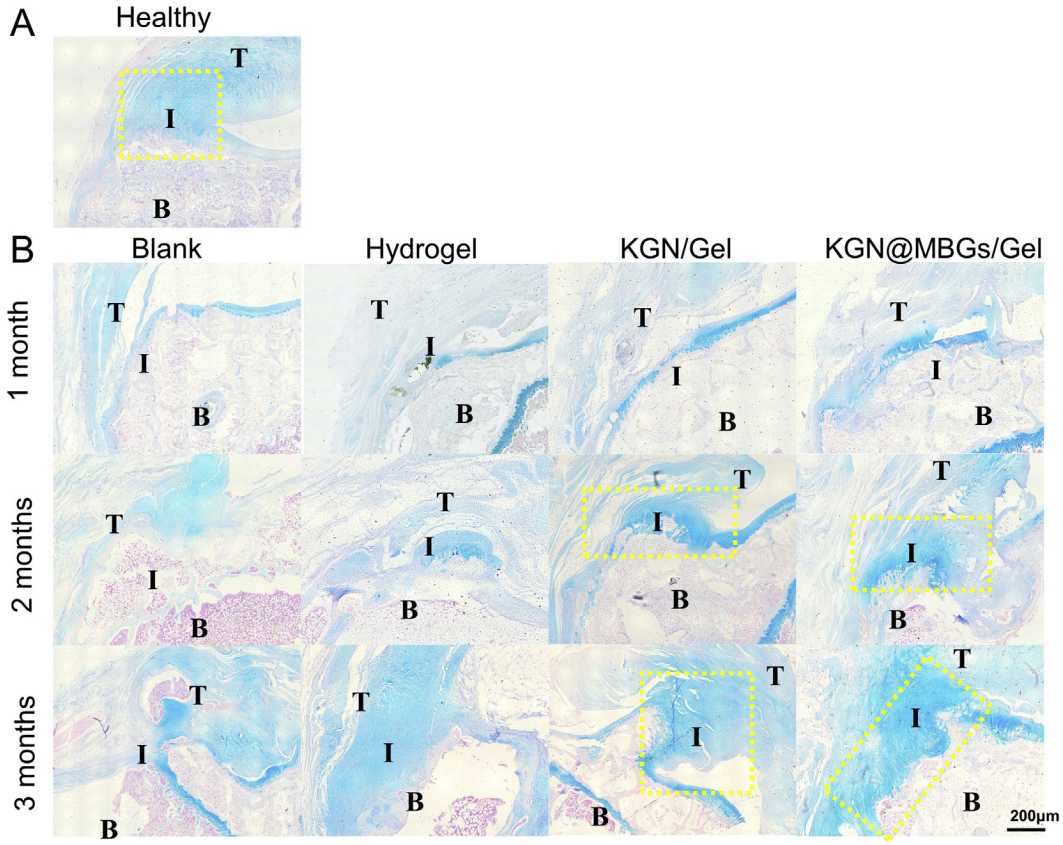

Fig. 8. Alcian blue staining results of the interface of tendon-to-bone. (**A**) The healthy interface showed abundant blue area (fibrocartilage layer) in TBJ. (**B**) Regeneration of cartilage layer (dark blue area) after repair without hydrogel or with simple hydrogel, KGN/Gel and KGN@MBGs/Gel for 1, 2, and 3 months. (T = tendon; B = bone; I = interface; the yellow box labeled the fibrocartilage area.). KGN, kartogenin; MBG, mesoporous bioactive glass nanoparticle; TBJ, tendon-bone junction.

for 2 weeks. A significant difference was observed in KGN@MBGs/Gel group by cell appearance and the OD value (Fig. 4C, blank: 0.443; simple hydrogel: 0.391; KGN/Gel: 0.435; KGN@MBGs/Gel: 0.880; $p < 0.001$). Fig. 4B showed the Alcian blue staining results of TDSCs after chondrogenic induction with different hydrogels for 3 weeks. Hydrogels with KGN showed benefits in cartilaginous pellets generation, which represented deeper stain, more extensive matrix and rounded cell morphology, thus got higher Bern score (Fig. 4D, blank: 5.33; simple hydrogel: 5; KGN/Gel: 8.33; KGN@MBGs/Gel: 8; $p < 0.05$).

Further experiment of differentiation-related protein expression was detected by WB. In process of osteogenic induction, Collagen I, Runx2, and BMP2 in KGN@MBGs/Gel group were proved to be up-regulated than other hydrogels without MBGs (Fig. 5A). While in chondrogenic induction, KGN/Gel and KGN@MBGs/Gel groups were found with higher expression of Collagen II, Sox9 and Aggrecan (Fig. 5B).

3.4. Effect of KGN@MBGs/Gel on TBJ healing of chronic RCTs

3.4.1. Bone loss after chronic RCTs

After 8 weeks of the detachment of the supraspinatus tendon, bone conditions of the greater tuberosity were confirmed by micro-CT. As shown in Fig. S5, trabecular bone of the greater tuberosity reduced significantly in the chronic RCTs group than that in sham groups. The BV/TV value was further proof of the significant bone loss as it was 47.87% in sham group but 40.6% in the chronic RCTs group ($p = 0.003$). So we successfully constructed the model of chronic RCT and proved the bone loss at the greater tuberosity [7].

3.4.2. Bone tunnel healing condition

For bone healing observation after hydrogels injection, reconstructed micro-CT images of the bone tunnel were used for comparison. Fig. 6A showed the example of the bone tunnel for suture fixation of the rotator cuff in sagittal, axial, and oblique axial view. As time went by, bone ingrowth conditions to the tunnel varied in different groups. KGN@MBGs/Gel started to show great superiority in bone regeneration of the enthesis from 2 months in reference to BV/TV values (Fig. 6B). Until 3 months, BV/TV value in KGN@MBGs/Gel group rose to 44.39% in the tunnel, even higher than the average value of the greater tuberosity of chronic RCTs model before repair surgery. Fig. 6C showed the longitudinal section of the bone tunnel for visible changes observation. There were still clear tunnels outline of the other three groups in 1 month except for the KGN@MBGs/Gel group. The margin became obscure from 2 months and more trabecular bones were observed in KGN@MBGs/Gel group. This phenomenon further confirmed the bone healing promotion effect of the hydrogels carrying MBGs.

3.4.3. Fibrocartilage layer regeneration in TBJ

Safranin O-fast green staining was widely used for TBJ observation owing to the pink dye in fibrocartilage while green dye in tendon and bone [38]. Fig. 7A showed the healthy TBJ of the sham group, in which a large area of fibrocartilage layer (pink) was observed. Tendon-bone healing conditions of different groups in 1,

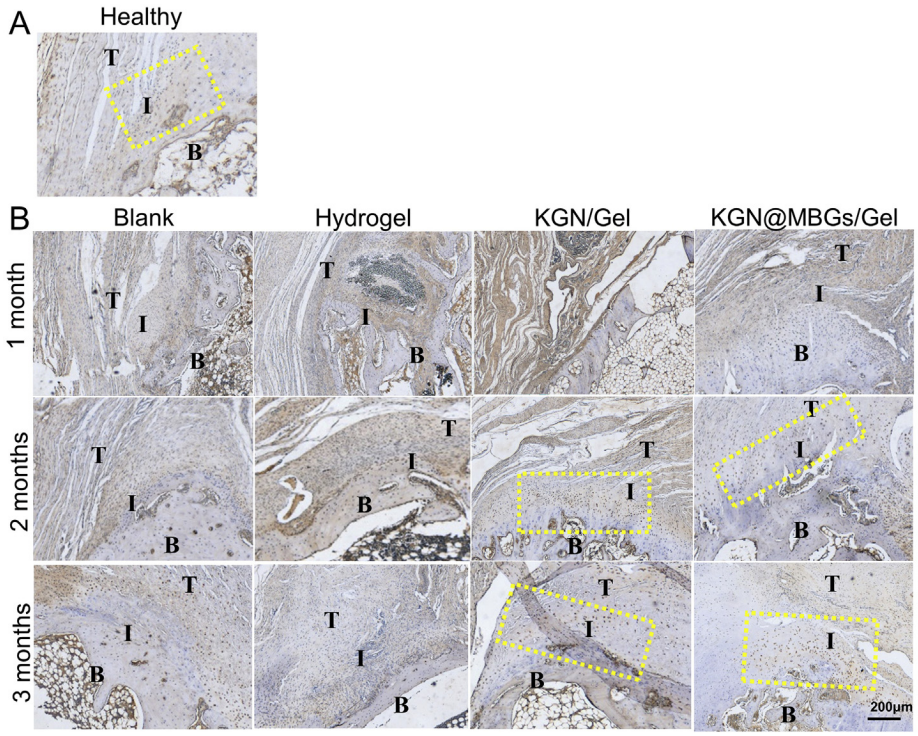

Fig. 9. Immunostaining of Col II results of the interface of tendon-to-bone. (**A**) The healthy interface showed Col II positive cells in interface. (**B**) Col II positive cells distribution in the interface of simple hydrogel, KGN/Gel, and KGN@MBGs/Gel for 1, 2, and 3 months. (T = tendon; B = bone; I = interface; the yellow box labeled the Col II positive cells.). KGN, kartogenin; MBG, mesoporous bioactive glass nanoparticle.

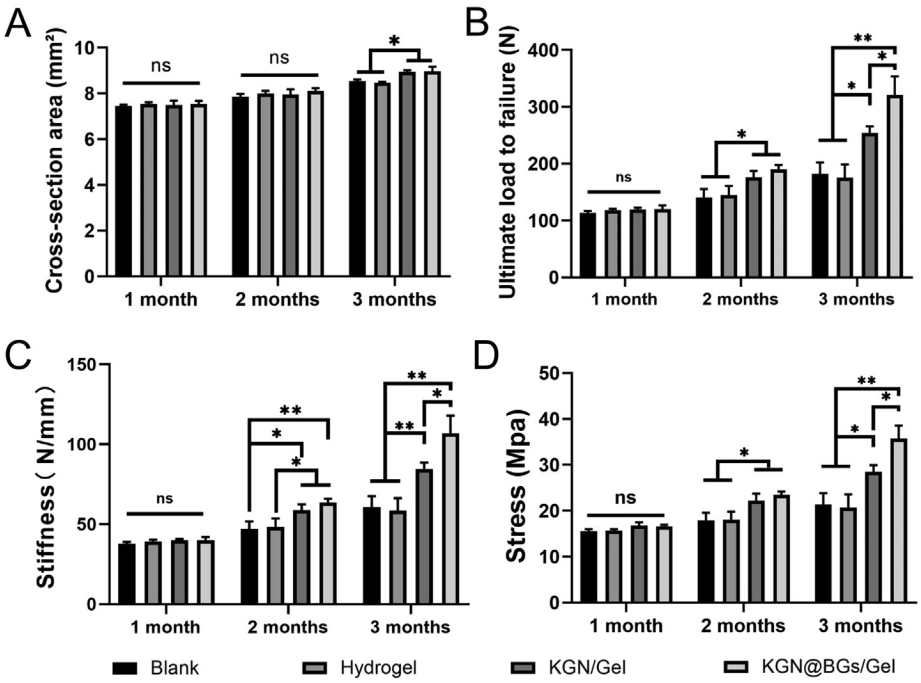

Fig. 10. Biomechanical test results of the supraspinatus tendon-humerus complex after rotator cuff repair with different hydrogels for 1, 2, and 3 months. (**A**) Cross-sectional area of tendon-bone junction. (**B**) Ultimate failure load, (**C**) stiffness, and (**D**) stress of the supraspinatus tendon-humerus complex. (*P < 0.05, **P < 0.01, n = 5).

2, and 3 months were presented in Fig. 7B. There were hardly tendon to bone connection in blank and hydrogel groups until 3 months. And no pink staining area was observed even in 3 months. Surprisingly, a tight junction of the tendon-to-bone and regenerated fibrocartilage layer appeared in TBJ of KGN/Gel and KGN@MBGs/Gel groups from 2 months. Similar results were observed in Alcian blue staining shown in Fig. 8. The regenerated fibrocartilage layer was dyed in blue because of the basophilic acid

mucopolysaccharide. Fig. 9 showed the Col II immunostaining results of TBJ. At the initial stage of repair, the positive area was mostly found at the extracellular matrix, but it decreased as healing progressed. After 2 months of repair, cells expressing intracellular collagen type II were found concentrated in TBJ of KGN/Gel and KGN@MBGs/Gel groups. This confirmed that the application of KGN with hydrogels is a benefit for fibrocartilage regeneration in the tendon-bone healing procedure.

3.4.4. Mechanical properties after rotator cuff repair

The supraspinatus and humerus complex was separated from surrounding tissues for biomechanical test after rotator cuff repair. As the TBJ healed, the cross-sectional area expanded gradually. There was a significantly larger cross-sectional area in groups with KGN than those without KGN in the TBJ after 3 months of repairing (Fig. 10A, $p < 0.05$). The ultimate load to failure, stiffness, and stress in KGN/Gel and KGN@MBGs/Gel groups grew faster than other groups from 2 months (Fig. 10B-C, $p < 0.05$). Hydrogels with BGs and KGN offered a longer-lasting effect than the other three groups so that mechanical property of the supraspinatus and humerus complex came to the highest in 3 months.

4. Discussion

In this study, the novel thermosensitive hydrogel was fabricated with the aim to promote tendon-to-bone healing of chronic rotator cuff tears. Several biochemical cues, including but not limited to growth factor (bone morphogenetic protein-2, connective tissue growth factor, and synthesis compounds such as KGN, were used to engineer the interface or entire integrated tissue [39,40]. In addition to the difficulty in reconstructing the fibrocartilage layer [41], bone loss at the enthesis may also lead to anchor loosening or pullout and eventually failure of RC repair [42,43]. This system, a combination of KGN and MBGs, had made great progress in curing bone loss and regenerating the fibrocartilage layer after the repairing of chronic RCTs. Besides evidence *in vivo*, an experiment *in vitro* further demonstrated the positive effect in osteogenesis and chondrogenesis differentiation of TDSCs. Figuratively speaking, this novel system acted as a facilitator of the TDSCs from the rotator cuff tendon for *in situ* healing.

The dilemma of repairing chronic RCTs has aroused widespread concern in the field of tissue engineering [44]. Various strategies have been applied to the treatment of chronic RCTs, including nanofiber scaffold [33], decellularized matrix scaffold [45], and biochemical factors injection [46]. However, some deficiencies still exist, including the complicated manufacturing process, non-persistent releasing, or undegradability. Thermosensitive MC-based hydrogels were first used in ophthalmic delivery [47]. This study, along with PVP, PVA and NaCl, has superiority of injectability and fluidity at room temperature, gel-forming property at body temperature. A similar property was reported by Bain using polyethylene glycol and NaCl [48]. After transosseous fixation of the rotator cuff tendon, the hydrogels could fill the tiny seam and work *in situ*, thus continuously releasing biochemical cues.

Mesenchymal stem cells transplantation is widely used in tissue engineering because of its multi-lineage differentiation characteristics; however, time-consuming or exclusive problems remain in the practical application [49,50]. Our system aimed to inspire TDSCs from the torn rotator cuff tendon and promote directional differentiation by improving the environment of the TBJ interface. Zhang et al. [51] found cartilage-like tissue formation induced by KGN injection (10 μL of 100 μmol/L) in the patella tendon, which proved the chondrogenesis inducing ability of KGN. Zhao et al. [52] confirmed the bone regeneration effect of MBGs by stimulating migration and differentiation of osteoprogenitor cells. Both KGN and MBGs were proved to enhance to proliferation capability of cells [19,21], which was consistent with our results. The KGN@MBGs/Gel system combined both of the advantages. Key genes expression of chondrogenesis and osteogenesis, Sox9 [53], and Runx2 [54], in TDSCs differentiation were found up-regulated, which proved the bi-lineage induction characteristics of this multifunctional system.

Healthy TBJ is protected by gradient construction from tendon to bone. So far in the clinic, surgery of rotator cuff repair could not help regenerate the transitional zone. KGN had been made progress in TBJ healing for it could enhance collagen organization and fibrocartilage formation [20,55]. Calcium deposition was beneficial for new bone generation at the enthesis [56]. In this study, KGN was grafted to MBGs and carried by thermosensitive hydrogels, so a total of 200 nM KGN would last longer in the interface, thereby made difference too. Besides *in vitro* experiments, we have demonstrated the effect of the KGN@MBGs/Gel system on transitional zone reconstruction *in vivo*. Immunohistological staining of Col II revealed that our system might promote regeneration of cells expressing intracellular collagen type II. These kinds of cells were believed to co-express collagen type I [57], thus improving TBJ healing.

Improvement of mechanical properties was shown in the humerus-tendon complex, which might be attributed to the following reasons: (1) biochemical clues *in situ* inspirated TDSCs from the rotator cuff stump to accelerate the healing process. (2) The gap of repaired tendon and bone was filled before the system gelled, which enabled cells to migrate and enlarged the cross-sectional area of TBJ. 3. The regeneration of the transition zone from fibrocartilage to bone could effectively conduct mechanical stimulation, reduce the stress concentration from tendon to bone and enhance the tissue bonding strength [4].

There still exist some limitations of our study. The major one is missing sham group after repair, for there might be some changes in healthy organs as time went by. Another one is the lack of groups using hydrogel with MBGs along. So it was difficult to analyze the interaction of KGN and MBGs.

5. Conclusion

Thermo-sensitive MC-based hydrogel carrying KGN@MBGs was successfully fabricated in this study, with sustained releasing of biochemical cues. This system has superiority in filling tiny cracks after tendon repairing to bone and gelating at body temperature. Furthermore, the bioactive factors were capable of inspiring TDSCs and promoting fibrocartilage and bone regeneration *in situ*, therefore accelerating transition zone healing of chronic RCTs and reversing bone loss condition. These bone and cartilage inductive capacities were confirmed *in vitro*, as the up-regulation of Runx2, bone morphogenetic protein-2, Collagen I, Sox9, Aggrecan and Collagen II were observed. Overall, we believe that KGN@MBGs/Gel therapy might be a valuable cell-free therapy, with promising application prospects in chronic RCTs.

Authors contributions

Kai Huang: Conceptualization; Data curation; Formal analysis; Investigation; Methodology; Project administration; Writing-original draft; Writing-review & editing; **Juan Du:** Conceptualization; Data curation; Formal analysis; Investigation;**Junjie Xu:** Data curation; Formal analysis; Investigation; **Chenliang Wu:** Data curation; Formal analysis; Methodology; **Sihao Chen:** Data curation; Formal analysis; Methodology; **Tonghe Zhu:** Funding acquisition; Supervision; **Jia Jiang;** Conceptualization; Funding acquisition; Supervision; Methodology;**Jinzhong Zhao:**

Conceptualization; Methodology; Investigation; Project administration; Resources; Supervision; Writing-review & editing.

Declaration of competing interest

The authors declare that they have no known competing financial interests or personal relationships that could have appeared to influence the work reported in this paper.

Acknowledgments

The authors sincerely appreciate the support of 'National Natural Science Foundation of China (Grant No. 81671920, 81871753, 81772341, 81902186)', 'National Key Research and Development Program of China (Grant No. 2018YFC1106200, 2018YFC1106201, 2018YFC1106202, 2018YFC1106203, 2018YFC1106204)', Shanghai Rising-Star Program (20QC1401300), and Science and Technology Commission of Shanghai Municipality (19441901700, 19441901701, 19441901702). The authors would like to thank TopEdit (www.topeditsci.com) for English language editing of this manuscript.

Appendix A. Supplementary data

Supplementary data to this article can be found online at https://doi.org/10.1016/j.mtchem.2021.100720.

References

[1] J. Guevara, V. Entezari, J. Ho, K. Derwin, J. Iannotti, E. Ricchetti, An update on surgical management of the repairable large-to-massive rotator cuff tear, J. Bone Jt. Surg. Am. 102 (19) (2020) 1742–1754.
[2] A. Colvin, N. Egorova, A. Harrison, A. Moskowitz, E. Flatow, National trends in rotator cuff repair, J. Bone Jt. Surg. Am. 94 (3) (2012) 227–233.
[3] L. Galatz, C. Ball, S. Teefey, W. Middleton, K. Yamaguchi, The outcome and repair integrity of completely arthroscopically repaired large and massive rotator cuff tears, J. Bone Jt. Surg. Am. 86 (2) (2004) 219–224.
[4] M. Raspanti, R. Strocchi, V. De Pasquale, D. Martini, C. Montanari, A. Ruggeri, Structure and ultrastructure of the bone/ligament junction, Ital. J. Anat Embryol. 101 (2) (1996) 97–105.
[5] L. Baldino, N. Maffulli, E. Reverchon, Bone–tendon Interface. Regenerative Engineering of Musculoskeletal Tissues and Interfaces, 2015, pp. 345–361.
[6] M. Hurtig, M. Buschmann, L. Fortier, C. Hoemann, E. Hunziker, J. Jurvelin, P. Mainil-Varlet, C. McIlwraith, R. Sah, R. Whiteside, Preclinical studies for cartilage repair: recommendations from the international cartilage repair society, Cartilage 2 (2) (2011) 137–152.
[7] M. Killian, L. Cavinatto, S. Shah, E. Sato, S. Ward, N. Havlioglu, L. Galatz, S. Thomopoulos, The effects of chronic unloading and gap formation on tendon-to-bone healing in a rat model of massive rotator cuff tears, J. Orthop. Res. 32 (3) (2014) 439–447.
[8] C. Yakacki, M. Poukalova, R. Guldberg, A. Lin, M. Saing, S. Gillogly, K. Gall, The effect of the trabecular microstructure on the pullout strength of suture anchors, J. Biomech. 43 (10) (2010) 1953–1959.
[9] L. Klouda, Thermoresponsive hydrogels in biomedical applications: a seven-year update, Eur. J. Pharm. Biopharm. 97 (2015) 338–349.
[10] E. Heymann, Studies on sol-gel transformations. I. The inverse sol-gel transformation of methylcellulose in water, Trans. Faraday Soc. 31 (1935).
[11] T. Bhunia, A. Giri, T. Nasim, D. Chattopadhyay, A. Bandyopadhyay, Uniquely different PVA-xanthan gum irradiated membranes as transdermal diltiazem delivery device, Carbohydr. Polym. 95 (1) (2013) 252–261.
[12] B. Niemczyk-Soczynska, A. Gradys, D. Kolbuk, A. Krzton-Maziopa, P. Sajkiewicz, Crosslinking kinetics of methylcellulose aqueous solution and its potential as a scaffold for tissue engineering, Polymers 11 (11) (2019).
[13] Abdel El-Naggar, M. Wahab, H. Helal, Reham, M. Senna, Magdy, Radiation synthesis and drug delivery properties of interpenetrating networks (IPNs) based on poly(vinyl alcohol)/methylcellulose blend hydrogels, Int. J. Biol. Macromol. 102 (2017) 1045–1051.
[14] C. Sunil Joshi, Sol-gel behavior of hydroxypropyl methylcellulose (HPMC) in ionic media including drug release, Materials 4 (10) (2011).
[15] M. Huanga, Y. Houa, Y. Lia, D. Wangb, L. Zhanga, High performances of dual network PVA hydrogel modified by PVP using borax as the structure-forming accelerator, Des. Monomers Polym. 20 (1) (2017) 505–513.
[16] K. Shimokawa, K. Saegusa, F. Ishii, Rheological properties of reversible thermo-setting in situ gelling solutions with the methylcellulose-polyethylene glycol-citric acid ternary system (2): effects of various water-soluble polymers and salts on the gelling temperature, Colloids Surf. B Biointerfaces 74 (1) (2009) 56–58.
[17] T. Campbell, P. Lapner, F. Dilworth, M. Sheikh, O. Laneuville, H. Uhthoff, G. Trudel, Tendon contains more stem cells than bone at the rotator cuff repair site, J. Shoulder Elbow Surg. 28 (9) (2019) 1779–1787.
[18] Q. Tan, P. Lui, Y. Rui, Y. Wong, Comparison of potentials of stem cells isolated from tendon and bone marrow for musculoskeletal tissue engineering, Tissue Eng. 18 (2012) 840–851.
[19] K. Johnson, S. Zhu, M. Tremblay, J. Payette, J. Wang, L. Bouchez, S. Meeusen, A. Althage, C. Cho, X. Wu, P. Schultz, A stem cell-based approach to cartilage repair, Science 336 (6082) (2012) 717–721.
[20] D. Wang, H. Tan, A. Lebaschi, Y. Nakagawa, S. Wada, P. Donnelly, L. Ying, X. Deng, S. Rodeo, Kartogenin enhances collagen organization and mechanical strength of the repaired enthesis in a murine model of rotator cuff repair, official publication of the Arthroscopy Association of North America and the International Arthroscopy Association, Arthrosc. J. Arthrosc. Relat. Surg. 34 (9) (2018) 2579–2587.
[21] X. Wang, W. Chen, Q. Liu, K. Gao, G. Wang, L. Gao, L. Liu, Function and mechanism of mesoporous bioactive glass adsorbed epidermal growth factor for accelerating bone tissue regeneration, Biomed. Mater. 12 (2) (2017) 25020.
[22] J. Chen, X. Chen, Z. Yang, X. Tan, J. Wang, Y. Chen, Preparation and characterization of folic acid functionalized bioactive glass for targeted delivery and sustained release of methotrexate, J. Biomed. Mater. Res. 107 (2) (2019) 319–329.
[23] A. Ulman, Formation and structure of self-assembled monolayers, Chem. Rev. 96 (4) (1996) 1533–1554.
[24] C. Chen, K. Huang, J. Zhu, Y. Bi, L. Wang, J. Jiang, T. Zhu, X. Yan, J. Zhao, A novel elastic and controlled-release poly(ether-ester-urethane)urea scaffold for cartilage regeneration, J. Mater. Chem. B 8 (18) (2020) 4106–4121.
[25] M. Bain, B. Bhowmick, D. Maity, D. Mondal, M. Mollick, B. Paul, M. Bhowmik, D. Rana, D. Chattopadhyay, Effect of PVA on the gel temperature of MC and release kinetics of KT from MC based ophthalmic formulations, Int. J. Biol. Macromol. 50 (3) (2012) 565–572.
[26] N. Saha, R. Shah, P. Gupta, B. Mandal, R. Alexandrova, M. Sikiric, P. Saha, PVP - CMC hydrogel: an excellent bioinspired and biocompatible scaffold for osseointegration, Mater. Sci. Eng. Mater. 95 (2019) 440–449.
[27] Y. Kanca, P. Milner, D. Dini, A. Amis, Tribological properties of PVA/PVP blend hydrogels against articular cartilage, J. Mech. Behav. Biomed. Mater. 78 (2018) 36–45.
[28] a.-l. kjøniksen, B. Nyström, Effects of polymer concentration and cross-linking density on Rheology of chemically cross-linked poly(vinyl alcohol) near the gelation threshold, Macromolecules 29 (15) (1996) 5215–5222.
[29] S. Zhao, J. Zhang, M. Zhu, Y. Zhang, Z. Liu, Y. Ma, Y. Zhu, C. Zhang, Effects of functional groups on the structure, physicochemical and biological properties of mesoporous bioactive glass scaffolds, J. Mater. Chem. B. 3 (8) (2015) 1612–1623.
[30] T. Ho, S. Tsai, S. Yeh, S. Chen, K. Tung, H. Chien, Y. Lu, C. Huang, Y. Tsao, PEDF-derived peptide promotes tendon regeneration through its mitogenic effect on tendon stem/progenitor cells, Stem Cell Res. Ther. 10 (1) (2019) 2.
[31] H. Su, R. Zheng, L. Jiang, N. Zeng, K. Yu, Y. Zhi, S. Shan, Dextran hydrogels via disulfide-containing Schiff base formation: synthesis, stimuli-sensitive degradation and release behaviors, Carbohydr. Polym. 265 (2021) 118085.
[32] S. Grogan, A. Barbero, V. Winkelmann, F. Rieser, J. Fitzsimmons, S. O'Driscoll, I. Martin, P. Mainil-Varlet, Visual histological grading system for the evaluation of in vitro-generated neocartilage, Tissue Eng. 12 (8) (2006) 2141–2149.
[33] W. Su, J. Guo, J. Xu, K. Huang, J. Chen, J. Jiang, G. Xie, J. Zhao, S. Zhao, C. Ning, Gradient composite film with calcium phosphate silicate for improved tendon -to-Bone intergration, Chem. Eng. J. 404 (2021) 126473.
[34] W. Su, W. Qi, X. Li, S. Zhao, J. Jiang, J. Zhao, Effect of suture absorbability on rotator cuff healing in a rabbit rotator cuff repair model, Am. J. Sports Med. 46 (11) (2018) 2743–2754.
[35] A. Inui, T. Kokubu, Y. Mifune, R. Sakata, H. Nishimoto, K. Nishida, T. Akisue, R. Kuroda, M. Satake, H. Kaneko, Regeneration of rotator cuff tear using electrospun poly(d,l-lactide-Co-glycolide) scaffolds in a rabbit model, Arthrosc. J. Arthrosc. Relat. Surg. 28 (12) (2012) 1790–1799.
[36] H.H. Winter, Can the gel point of a crosslinking polymer be detected by the G'-G" crossover? Polym. Eng. Sci. 27 (22) (2010) 1698–1702.
[37] Z. Li, X. Zhang, J. Ouyang, D. Chu, F. Han, L. Shi, R. Liu, Z. Guo, G. Gu, W. Tao, L. Jin, J. Li, Ca-supplying black phosphorus-based scaffolds fabricated with microfluidic technology for osteogenesis, Bioact. Mater. 6 (11) (2021) 4053–4064.
[38] W. Song, Z. Ma, C. Wang, H. Li, Y. He, Pro-chondrogenic and immunomodulatory melatonin-loaded electrospun membranes for tendon-to-bone healing, J. Mater. Chem. B 7 (42) (2019) 6564–6575.
[39] P.J. Yang, J.S. Temenoff, Engineering orthopedic tissue interfaces, Tissue Eng. B Rev. 15 (2) (2009) 127–141.
[40] D. Wang, X. Zhang, S. Huang, Y. Liu, F. Dai, Engineering multi-tissue units for regenerative medicine:bone-tendon-muscle units of the rotator cuff, 10100, Biomaterials (2021) 120789.
[41] T.M. Campbell, L. Gao, O. Laneuville, H. Louati, H.K. Uhthoff, G. Trudel, Rotator cuff anchor repair: histological changes associated with the recovering mechanical properties in a rabbit model, J. Tissue Eng. Regen. Med. 15 (6) (2021) 567–576.
[42] S. Chung, J. Oh, H. Gong, J. Kim, S. Kim, Factors affecting rotator cuff healing after arthroscopic repair: osteoporosis as one of the independent risk factors, Am. J. Sports Med. 39 (10) (2011) 2099–2107.
[43] T. Thangarajah, F. Henshaw, A. Sanghani-Kerai, S. Lambert, C. Pendegrass, G. Blunn, Supraspinatus detachment causes musculotendinous degeneration and a reduction in bone mineral density at the enthesis in a rat model

of chronic rotator cuff degeneration, Shoulder Elbow 9 (3) (2017) 178–187.
[44] S. Patel, A. Gualtieri, H. Lu, W. Levine, Advances in biologic augmentation for rotator cuff repair, Ann. N. Y. Acad. Sci. 1383 (1) (2016) 97–114.
[45] J. Neumann, M. Zgonis, K. Rickert, K. Bradley, T. Kremen, B. Boggess, A. Toth, Interposition dermal matrix xenografts: a successful alternative to traditional treatment of massive rotator cuff tears, Am. J. Sports Med. 45 (6) (2017) 1261–1268.
[46] S. Shah, I. Kormpakis, N. Havlioglu, M. Ominsky, L. Galatz, S. Thomopoulos, Sclerostin antibody treatment enhances rotator cuff tendon-to-bone healing in an animal model, J. Bone Jt. Surg. Am. 99 (10) (2017) 855–864.
[47] V. Gugleva, S. Titeva, N. Ermenlieva, S. Tsibranska, D. Momekova, Development and evaluation of doxycycline niosomal thermoresponsive in situ gel for ophthalmic delivery, Int. J. Pharm. 591 (2) (2020) 120010.
[48] M.K. Bain, M. Bhowmik, D. Maity, N.K. Bera, S. Ghosh, D. Chattopadhyay, Control of thermo reversible gelation of methylcellulose using polyethylene glycol and sodium chloride for sustained delivery of ophthalmic drug, J. Appl. Polym. Sci. 118 (2) (2010) 631–637.
[49] C. Chiang, Y. Fang, C. Ho, M. Assunção, S. Lin, Y. Wang, A. Blocki, C. Huang, Bioactive decellularized extracellular matrix derived from 3D stem cell spheroids under macromolecular crowding serves as a scaffold for tissue engineering, Adv. Healthc. Mater. 10 (11) (2021) e2100024.
[50] J. Huang, Z. Huang, Y. Liang, W. Yuan, L. Bian, L. Duan, Z. Rong, J. Xiong, D. Wang, J. Xia, 3D printed gelatin/hydroxyapatite scaffolds for stem cell chondrogenic differentiation and articular cartilage repair, Biomater. Sci. 9 (7) (2021) 2620–2630.
[51] J. Zhang, J. Wang, Kartogenin induces cartilage-like tissue formation in tendon-bone junction, Bone Res. 2 (2014).
[52] F. Zhao, W. Xie, W. Zhang, X. Fu, W. Gao, B. Lei, X. Chen, 3D printing nanoscale bioactive glass scaffolds enhance osteoblast migration and extramembranous osteogenesis through stimulating immunomodulation, Adv. Healthc. Mater. 7 (16) (2018) e1800361.
[53] M. Caron, M. Eveque, B. Cillero-Pastor, R. Heeren, B. Housmans, K. Derks, A. Cremers, M. Peffers, L. van Rhijn, G. van den Akker, T. Welting, Sox9 determines translational capacity during early chondrogenic differentiation of ATDC5 cells by regulating expression of ribosome biogenesis factors and ribosomal proteins, Front. Cell Dev. Biol. 9 (2021) 686096.
[54] Q. Dai, Z. Xu, X. Ma, N. Niu, S. Zhou, F. Xie, L. Jiang, J. Wang, W. Zou, mTOR/Raptor signaling is critical for skeletogenesis in mice through the regulation of Runx2 expression, Cell Death Differ. 24 (11) (2017) 1886–1899.
[55] Y. Zhou, J. Zhang, J. Yang, M. Narava, G. Zhao, T. Yuan, H. Wu, N. Zheng, M. Hogan, J. Wang, Kartogenin with PRP promotes the formation of fibrocartilage zone in the tendon-bone interface, J. Tissue Eng. Regen. Med. 11 (12) (2017) 3445–3456.
[56] D. Kovacevic, A. Fox, A. Bedi, L. Ying, X. Deng, R. Warren, S. Rodeo, Calcium-phosphate matrix with or without TGF-β3 improves tendon-bone healing after rotator cuff repair, Am. J. Sports Med. 39 (4) (2011) 811–819.
[57] A. Tekari, R. Luginbuehl, W. Hofstetter, R. Egli, Chondrocytes expressing intracellular collagen type II enter the cell cycle and co-express collagen type I in monolayer culture, official publication of the Orthopaedic Research Society, J. Orthop. Res. 32 (11) (2014) 1503–1511.